New experimental measurement of ^{nat}Er(n, γ) cross sections between 1 and 100 eV

X. X. Li,[1,2] L. X. Liu,[2,3] W. Jiang,[4,5] J. Ren,[6] H. W. Wang,[3,1,2,*] G. T. Fan,[3,1,2,†] X. G. Cao,[3,1,2] Y. Zhang,[4,5] X. R. Hu,[1,2] Z. R. Hao,[1,2] P. Kuang,[1,2] B. Jiang,[1,2] X. H. Wang,[2] J. F. Hu,[2] J. C. Wang,[7] D. X. Wang,[7] S. Y. Zhang,[7] Y. D. Liu,[8] X. Ma,[8] C. W. Ma,[9] Y. T. Wang,[9] Z. D. An,[2,10] J. J. He,[11] J. Su,[11] L. Y. Zhang,[11] Y. X. Yang,[2,12] W. B. Liu,[2,9] and W. Q. Su[2,9]

[1]*University of Chinese Academy of Sciences, Beijing 100049, China*
[2]*Shanghai Institute of Applied Physics, Chinese Academy of Sciences, Shanghai 201800, China*
[3]*Shanghai Advanced Research Institute, Chinese Academy of Sciences, Shanghai 201210, China*
[4]*Institute of High Energy Physics, Chinese Academy of Sciences, Beijing 100049, China*
[5]*China Spallation Neutron Source, Dongguan 523803, China*
[6]*China Institute of Atomic Energy, Beijing 102413, China*
[7]*Institute of Nuclear Physics, Inner Mongolia University For The Nationalities, Tongliao 028000, China*
[8]*Xiangtan University, Xiangtan 411105, China*
[9]*Henan Normal University, Xinxiang 453007, China*
[10]*Sun Yat-sen University, Zhuhai 510275, China*
[11]*Beijing Normal University, Beijing 100875, China*
[12]*School of Physics and Microelectronics, Zhengzhou University, Zhengzhou 450052, China*

(Received 30 June 2021; accepted 30 September 2021; published 3 November 2021)

^{162}Er and ^{164}Er are two of the 35 p nuclei, and their (n, γ) cross sections are important input parameters in nuclear astrophysics network calculations. The neutron capture cross section in the resonance region of isotopes and even the natural erbium (^{nat}Er) sample has not been measured experimentally according to the EXFOR database. The (n, γ) cross section of ^{nat}Er, using C_6D_6 liquid scintillator and pulse height weighting techniques to measure prompt γ rays, has been measured in the energy range of 1–100 eV using a back streaming white neutron facility at China Spallation Neutron Source. The deduced neutron capture cross sections matches the evaluation databases ENDF/B-VIII.0, ENDF/B-VII.1, JENDL-4.0, and ROSFOND-2010, and resonance parameters extracted from the R-matrix code in the 1–100 eV region.

DOI: 10.1103/PhysRevC.104.054302

I. INTRODUCTION

Elemental abundances above iron are primarily produced by two distinct neutron capture processes in stars and stellar explosions, i.e., the slow neutron capture process (s process) [1] and the rapid neutron capture process (r process) [2]. Approximately, only 1% of heavy element abundances are produced by charged particles and photoinduced reactions (p process) [3]. The s process involves a series of neutron capture reactions in stars, particularly asymptotic giant branch stars [4], and is responsible for producing approximately half of all elements heavier than iron. The seed nucleus of the s process undergoes neutron capture reactions to form high atomic number isotopes. If the new isotope is stable, it will capture further neutrons and produce increasingly heavier isotopes. However, if the generated isotope is unstable, it will produce an isotope with the same mass number but different atomic number by β decay. Because of the extremely high neutron flux involved, the r process produces highly unstable neutron-rich nuclei [5]. Nuclei between ^{74}Se and ^{196}Hg cannot be synthesized by any known neutron capture process. They contain more protons than other stable isotopes [6]. Such nuclides are called p nuclei because the p process is responsible for their synthesis (see Fig. 1 for details). In principle, p nuclei can be produced by three reactions: proton capture, photonuclear reactions, and neutrino-driven nuclear reactions.

Natural erbium has six stable isotopes. ^{166,167,168}Er are the isotopes produced by the s process, and ^{170}Er is produced by the r process. Their (n, γ) cross sections are of great significance for understanding the pathways taken during the s process. It is worth noting that ^{162}Er and ^{164}Er are considered p nuclei in nuclear astrophysics. They are not produced by neutron capture but rather carry out (n, γ) reactions, the measurement of which can help us to better understand the results of relevant photonuclear reaction experiments.

For natural erbium, $S_n = 6.4928\,\text{MeV}$, $N_s = 0.9006\,\text{g/cm}^3$, $N = 0.0538 \times N_A/\text{cm}^3$ (N_A is Avogadro's constant), $t = 0.1$ cm The neutron capture cross section σ_c and neutron total cross section σ_t of natural erbium is calculated according to the σ_c and σ_t values of different isotopes (data from evaluation databases) and their corresponding abundance weights (as shown in Fig. 2).

Until now, there has not been enough experimental data for the erbium element in the 1–100 eV resonance energy region,

*Corresponding author: wanghongwei@zjlab.org.cn
†Corresponding author: fangongtao@zjlab.org.cn

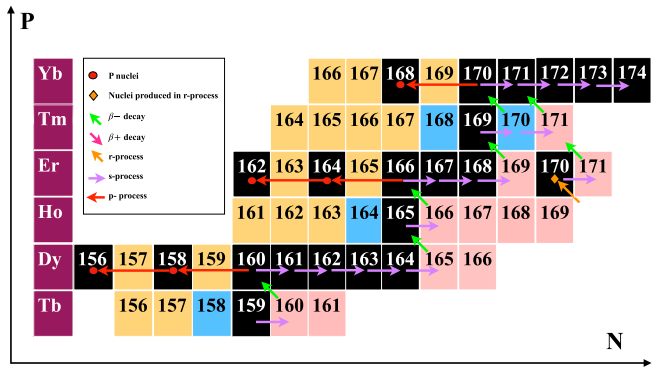

FIG. 1. The main nucleosynthesis path for ^{nat}Er in massive stars. Black boxes represent stable isotopes; yellow, blue, and red boxes represent unstable isotopes. Yellow color indicates that the nucleus decays via EC; red indicates decay via β decay; while blue indicates that the nucleus decays via both EC and β decay.

except for keV energy [7] and the thermal neutron energy region [8–10]. Haddad *et al.* measured the neutron capture cross section of natural erbium at 0.01 eV–10 eV in 1963, given the first resonance peak of natural erbium [11].

The China spallation neutron source (CSNS) is mainly used for the experimental study of neutron scattering [12–15]. The back streaming white neutron facility (Back-n), built in the beginning of 2018 [16], is a branch line of the CSNS [12]. It is the first spallation neutron time-of-flight facility in China, and it is mainly used for neutron nuclear data measurements. The maximum neutron flight distance of Back-n is approximately 80 m, while the neutron energy range is 0.5 eV–200 MeV. At the Back-n experimental station, the neutron flux can reach 10^7 cm^{-2}s^{-1}. When the proton accelerator operates in single bunch mode, the neutron time resolution at 80 m from the spallation target in the energy region of 0.2 eV–2.8 MeV is approximately 0.80% [17,18].

This work is the first experimental measurement of neutron capture cross section of natural erbium in the energy region between 1 eV and 100 eV at the Back-n facility at the CSNS.

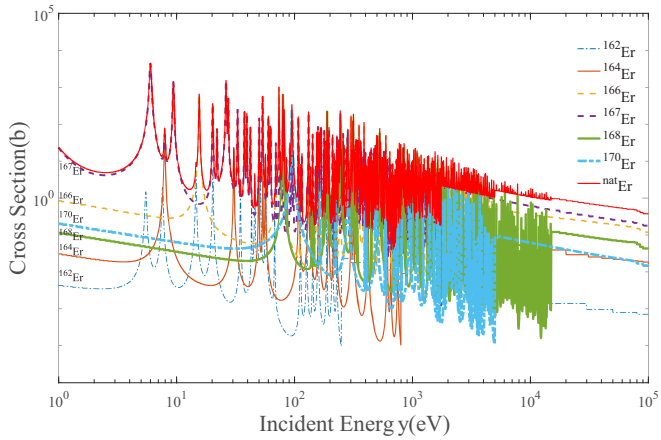

FIG. 2. The neutron cross section σ_c of natural erbium calculated by their isotopes capture cross section σ_c and was normalized by their abundance weights.

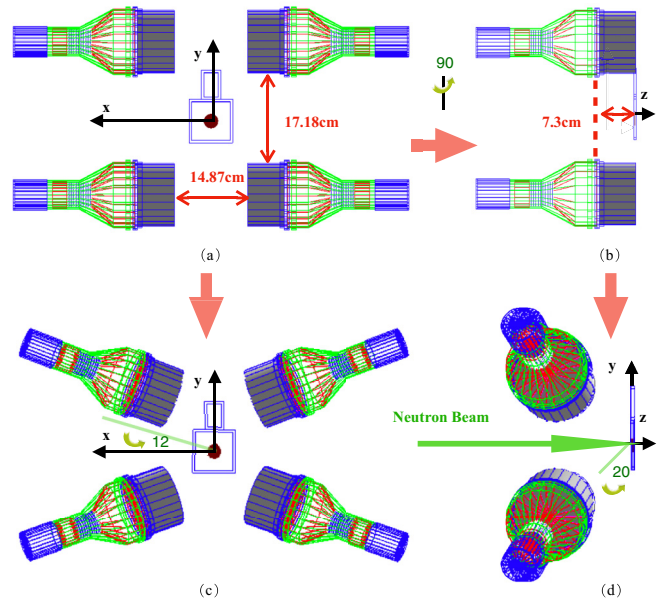

FIG. 3. Relative positions and setup of the detectors. (a) Detector distance is 14.87 cm and 17.18 cm in plane setup. (b) The detector PMT plane to target is 7.3 cm. (c),(d) Rotate the x axis by 12 degrees and the y axis by 20 degrees to get the final detector layout

Experimental data for the range of 30–100 keV are compared with existing experimental data, since small deviations can demonstrate the validity of the results. The experimental methods and data processing and uncertainty are analyzed in detail below. The neutron capture resonance parameters of natural erbium in this energy region are also provided.

II. EXPERIMENTAL METHOD

A detection system consisting of four C_6D_6 scintillation detectors was installed at the center of ES#2, approximately 76 m away from the spallation target and the four C_6D_6 detectors (EJ-315) were closely arranged using an aluminum holder. The C_6D_6 liquid scintillator was 127 mm in diameter and 76.2 mm in length, the scintillator was contained in a 1.5 mm thick aluminum capsule and coupled with a photomultiplier tube (ETEL 9390 KEB PMT) [19]. The detector is designed to measure emitted γ rays and to reduce neutron response. Consequently, a backward detector layout is shown in Fig. 3. The neutron flux was measured using a silicon monitor, which is based on the ^{6}Li$(n, \alpha)^3$H reaction [20]. Anode signals delivered by PMTs were recorded by the Back-n general-purpose data acquisition system (DAQ), which adopts full waveform data acquisition solution. The DAQ was triggered by the 25 Hz proton signal from the CT signal [21], then, all arrival signals calculated by prompt γ rays recorded by a digitizer with sampling rate of 1 Gs/s and 12-bit resolution. All data analyses were performed offline [22].

The experimental time about 105 h, for gold (^{197}Au), carbon (^{nat}C), and natural erbium (^{nat}Er) target detail information are shown in Table I. We detected the isotope abundance of the target and shown in Table II. The gold target (^{197}Au), as

TABLE I. Information of experimental targets.

Material	Formula	Diameter	Thickness	Mass
^{nat}Er	Er > 99.742% Gd = 0.018% Tm <0.005% Fe <0.050% Mg <0.050% Ni <0.050% Si = 0.012% C <0.010% W = 0.035% Ca = 0.023% Tb <0.005% Eu <0.010% Dy <0.020% Sm = 0.010% Yb = 0.010%	50.000(±0.001) mm	1.000(±0.001) mm	4.565(±0.001) g
^{nat}C	C >99.900%	50.000(±0.001) mm	1.000(±0.001) mm	4.583(±0.001) g
^{197}Au	Au >99.900%	30.000(±0.001) mm	1.000(±0.001) mm	13.768(±0.001) g

a standard neutron capture cross section, was measured for 13 h in proton power between 50.5 and 51.9 kW to check the experimental setup and DAQ [23]. Subsequently, the natural erbium target was measured for 72 h in beam power 50.5–51.5 kW then measured 8 h of empty target data and carbon target was 12 h. A total data of ≈8 TB were accumulated during the whole experiment.

III. DATA ANALYSIS

Due to the complex de-excitation path of the neutron capture compound nucleus, the C_6D_6 detector layouts are based on the assumption that only one de-excited γ ray is measured in the experiment, that is, the pulse height weighting technique (PHWT) [24], of which the detection efficiency is independent of the energies of cascade γ rays [25,26].

Experimental capture yields were obtained by means of weighting function (WF), which is parametrized as polynomial functions of the γ-ray energy. WF be express as

$$WF(E_d) = \sum_{i=0}^{4} a_i E_d^i, \tag{1}$$

where the WF is the weight function, E_d is an energy bin of pulse height spectrum, a_i is the parameters of the weight function, and can be determined by least squares method fit:

$$\chi^2 = \sum (kE_{\gamma j} - \int_{EL}^{\infty} R(E_d, E_{\gamma j}) WF(E_d) dE_d)^2, \tag{2}$$

where the $E_{\gamma j}$ is the energy of γ ray of group j, $R(E_d, E_{\gamma j})$ are counts of the pulse height (PH) spectrum with energy response function in E_d, EL is the threshold of PH spectrum. Here, we set the coefficient $k = 1$. Each event is weighed by the proper WF to ensure that the detector weighted efficiency is proportional to their excitation energy as shown in Fig. 4. This raw data manipulation is valid when the original efficiency is sufficiently low as only one γ ray per capture event is measured in the C_6D_6 setup [27,28].

The energy deposition for different monoenergetic γ rays in the C_6D_6 detector layout, as shown in Fig. 3, was simulated using the GEANT4 Monte Carlo program [29]. The original efficiency curve is shown in Fig. 4(a). Applying the weight function to the original efficiency curve, the linear relationship between detection efficiency and energy is shown in Fig. 4(b), and the ratio of efficiency to energy in Fig. 4(c) is approximately equal to 1.

After applying WFs, the capture yield (Y_w) can be determined using the following formula:

$$Y_w(E) = \frac{N_w}{N_s I S_n}, \tag{3}$$

where N_w is the weighted PH spectrum count, N_s is the sample area density, S_n is the target neutron binding energy, and I is the neutron flux provided by Back-n neutron monitor [30]. The relationship between the neutron capture cross section and the reaction yield is as follows:

$$Y_w(E) = (1 - e^{N\sigma_t(E)t f_c}) \frac{\sigma_c(E)}{\sigma_t(E)}, \tag{4}$$

where σ_c is the neutron capture cross section, σ_t is the neutron total cross section, N is the atom density, and t is the target thickness. Owing to the multiple scattering effect in a thick target, a correction factor f_c is introduced in calculation.

TABLE II. Isotope abundance of the target Er

Isotope	^{162}Er	^{164}Er	^{166}Er	^{167}Er	^{168}Er	^{170}Er
Target abundance	0.139	1.606	33.503	22.869	26.940	14.943
Natural abundance	0.139	1.601	33.503	22.869	26.978	14.910

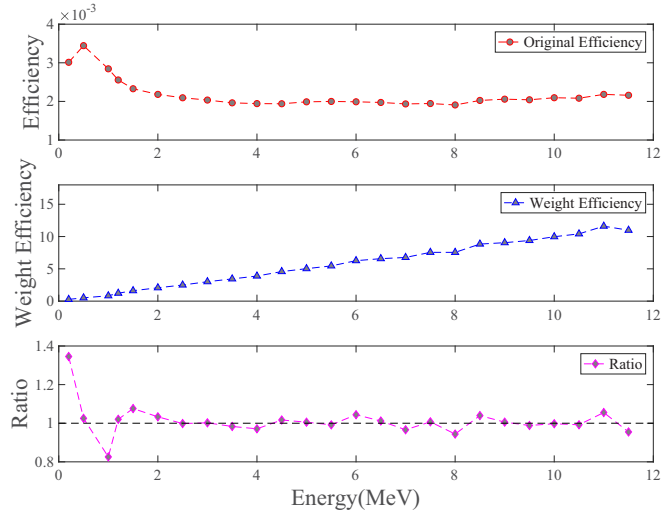

FIG. 4. (a) The C_6D_6 original efficiency. (b) Weighted efficiency. (c) The ratio of weighted efficiency to γ ray energy. For below 1.5 MeV, the weighted efficiency is not proportional to the energy to eliminate the influence of the weight function failure by setting a threshold when processing the PH spectrum.

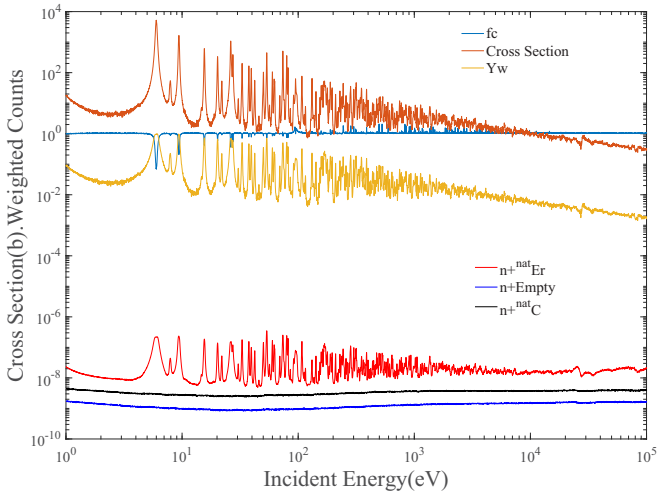

FIG. 5. The capture cross section, capture yield, target thickness correction factor (f_c) in the top and counting yield of the natural erbium target, empty, and carbon target (normalized to the neutron flux rate) in the bottom.

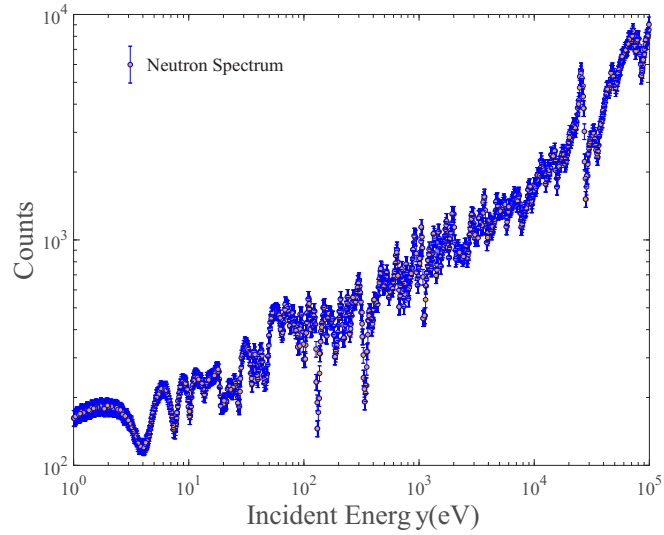

FIG. 6. Neutron spectrum in Back-n ES#2

GEANT4 simulations were used to determine the value of f_c (as seen in Fig. 5). Overall, the f_c value with neutron energy tends to be stable, there is a clear decrease in the energy near 6 eV, because the Er neutron absorption cross section a significant increased at this energy point. The neutron capture cross section of the sample can then be expressed using the following formula:

$$\sigma_c = \frac{N_w}{N_s I S_n} \times \frac{\sigma_t}{1 - e^{N\sigma_t f_c t}}. \tag{5}$$

The experimental error includes statistical and system errors, which are mainly from the following contributions, i.e., experimental conditions uncertainty, data analysis method uncertainty, and experimental statistical error (see Table III for details). Experimental conditions uncertainty depends on the experimental conditions including uncertainty of energy spectrum and the proton beam power. According to the Back-n collaboration [30], the uncertainty of the energy spectrum is between 2.30% and 4.50% above 0.15 MeV and less than 8.00% below 0.15 MeV. The neutron spectrum in Back-n ES#2 is shown in Fig. 6. Uncertainty proton beam power was recorded during the measurement, resulting in an uncertainty of 2.20%.

Uncertainties in data analysis are mainly caused by the PHWT method, background subtraction, and normalization process. Since the measurement of the neutron capture cross section using pulse height weight techniques is based on simulations, the details of the experimental environment and the PWHT method [23] simulation will affect the uncertainty estimation. However, the upper cascade γ cannot be ignored, it has approximately 1.00% uncertainty. At the same time, the emission of internal conversion electrons (EC) may lead to a reduction in the cascade γ count, a cascade γ emission program including a simplified model of the internal conversion process is used in the simulation (<0.5%). Previously, Tain *et al.* compared the neutron width PHWT treatment results of a 1.15 keV formant in ^{56}Fe with experimental results, finding that the systematic error of PHWT was 2.00%–3.00% [31]. After calculating the neutron capture cross section according to formula (5), the first resonant peak (5.734 eV) was used to normalize the low energy results because the proton beam

TABLE III. The statistical error and systematic error of the experiment

σ	Meaning	Value
	Experimental conditions	
σ (Beam power)	Uncertainty from beam power	<1.98%
$\sigma(I_1)$	Uncertainty from energy spectra above 0.15 MeV	<4.50%
$\sigma(I_2)$	Uncertainty from energy spectra below 0.15 MeV	<8.00%
	Data analysis	
σ (PHWT)	Uncertainty from PHWT method	<3.00%
σ (Normalized)	Uncertainty from normalized	<1.00%
σ (In beam)	Uncertainty from counts of in-beam BKG	<6.51%
$\sigma(T)$	Uncertainty from target parameters	<0.10%
	Statistical error	
σ (Statistic)	Uncertainty from mathematical statistics	<0.18%

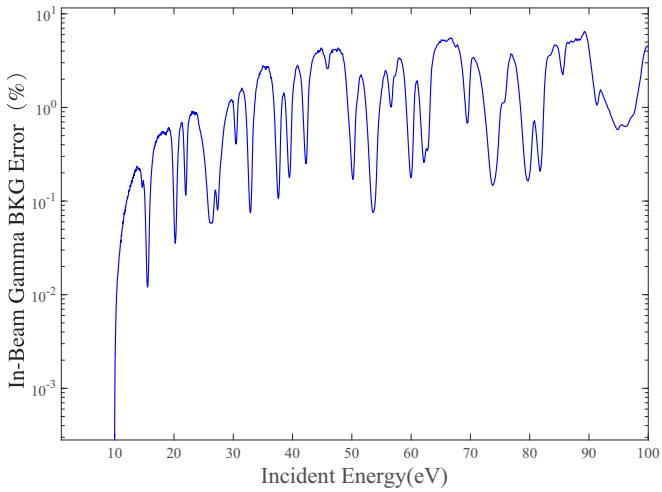

FIG. 7. The contribution of the in-beam γ background to the error of the Er target experimental results.

power fluctuation is not considered in the neutron energy spectrum. Two methods are considered in the normalization process: one is a Gaussian fitting of the experimental first resonance peak of 5–7 eV, in which the normalized coefficient is calculated by comparing the fitted curve width against the evaluation data, and the other involves a comparison with evaluation data according to the experimental energy bin, selecting the energy bin in 5–7 eV, then calculating the normalized coefficient. The calculation of the normalization coefficient contributed an error less than 1.00%.

According to recent studies using the Back-n facility [22,32], there is an obvious in-beam γ background between 20 μs and 400 μs (keV energy region).The Back-n collaboration published the measurement results of the in-beam γ background in 2020. We used this result and normalized it to our experimental conditions. Using the ratio of the Er target counts to the in-beam γ background counts, we obtained the contribution of the in-beam γ background to the error of the Er target experimental results, as shown in Fig. 7. The results show that in the energy range between 1 and 100 eV, the maximum contribution of the beam background to the error of the Er target experimental measurement result is 6.508% at the energy of 89.228 eV.

Uncertainty in data analysis also includes the systematic uncertainty caused by the cross-section process. The measurement of target parameters will cause this uncertainty, as is shown in Table II, it is less than 0.03%.

Finally, the statistical uncertainty of the experiment was 0.18%.

The data and uncertainty analysis in the region of 1–100 eV and 10–100 keV refers to the above method. However, we miss the in-beam γ background data at the energy region between 100 eV to 10 keV, regarding this part of the data, we regret that this work cannot give a detailed uncertainty.

IV. RESULT AND DISCUSSION

The neutron capture cross section of a natural erbium target was measured for the first time in the resonance energy range

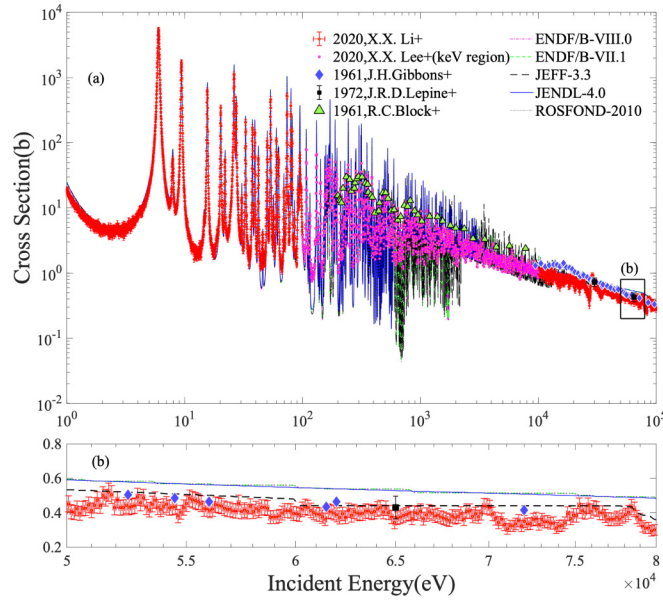

FIG. 8. (a) The experimental data were compared with existing experimental data and evaluation data in the range of 0.1–100 keV to evaluate their validity. (b) In the 50–80 keV energy region, the results of the three experiments are closer to those of JEFF-3.3, but significantly lower than those of the other evaluation databases considered.

of 1 eV–100 eV, and analyzed by the PWHT method and compared with those existing experimental data in 10–100 keV, as shown in Fig. 8(a). In the 10–100 keV region, the new data show a good agreement with some evaluation data and existing experimental data, if a more accurate response function of the beam-line can be obtained, the experiment results will be greatly improved.

It can be seen from Fig. 8(b), in the 50–80 keV energy, three sets of experimental data are basically the same, and the experimental data are all lower than the evaluation database of ENDF/B-VIII.0, ENDF/B-VII.1,JENDL-4.0, and ROSFOND-2010. But it is in good agreement with the evaluation data trend of JEFF-3.3.

The neutron capture cross sections between 1–100 eV energy were analyzed using the *R*-matrix SAMMY code [33] which takes into account all experimental effects, such as multiple interaction events (multiple scattering), self-shielding, the broadening of resonances due to thermal motion (Doppler broadening), and the resolution of the experimental setup. In addition, the full sample composition, including impurities, was taken into account [34–36] in simulation. There are some individual resonance parameters, such as resonance spin $\boldsymbol{J}$, neutron, and radiative partial decay widths Γ_n and Γ_γ, that can be determined in the fitting data. In general, only energy and capture kernel k, defined as

$$k = g\frac{\Gamma_n\Gamma_\gamma}{\Gamma_n + \Gamma_\gamma}, \tag{6}$$

can be obtained reliably. The statistical factor g is given by

$$g = \frac{2\boldsymbol{J}+1}{(2\boldsymbol{s}+1)(2\boldsymbol{I}+1)}, \tag{7}$$

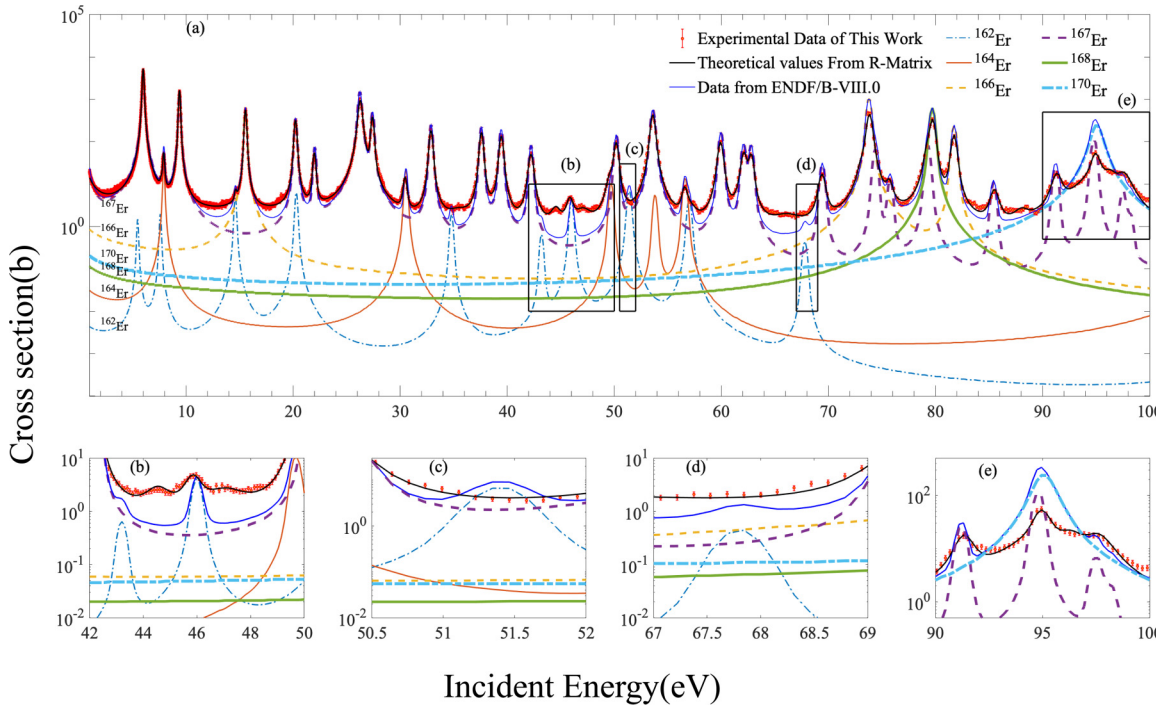

FIG. 9. (a) Resonance fits of the experimental data (solid symbols with error bars). Blue curve represents the evaluated data listed in the ENDF/B-VIII.0 database, and black curve shows the present fits. Dotted lines represent the contribution of isotopes. (b) The experimental data show that there is a resonance structure near 44.506 eV and 47.086 eV; the former may be contributed by ^{162}Er, but we cannot find an obvious source for the latter. (c),(d) ^{162}Er has a resonance structure at 51.4 eV and 67.8 eV, but there is no clear resonance peak in the experimental data. (e) There is a resonance structure near 87.875 eV, which is contributed by ^{170}Er, but we cannot identify a clear source.

where $s = 1/2$ is the neutron spin, $\boldsymbol{I}$ is the ground state spin of the target nucleus. $\boldsymbol{J} = |\boldsymbol{L} + \boldsymbol{S}|$, $\boldsymbol{S} = \boldsymbol{s} + \boldsymbol{I}$, $\boldsymbol{L}$ is the orbital angular momentum. The final fitted capture cross sections are shown in Fig. 9 and the extracted resonance parameters are listed in Table IV.

The experimental data show that there is a weak resonance structure near 44.506 eV, as shown in Fig. 9(b). The analysis shows that it is the contribution of the ^{162}Er resonance peak. The *R* matrix program FITTING shows that, except for the contribution of ^{162}Er at 45.846 eV, the two nearby faint bumps are not real resonance peaks, but are formed due to the superposition of the contributions of the direct capture cross sections of different isotopes. In addition, according to the ENDF evaluation database parameters, ^{162}Er should have the weak resonance peaks at 51.4 eV in Fig. 9(c), and 67.8 eV in Fig. 9(d), but there is no obvious resonance structure to be found in experimental data, this may be due to the low abundance of ^{162}Er, and the contribution of this resonance is weaker than the direct capture cross section of other isotopes, so it was not shown in the experimental data. The resonance peak at 90–100 eV [shown as Fig. 9(e)] is mainly composed of three narrow resonances of ^{162}Er and a wide resonance of ^{170}Er. Starting from this energy region, the influence of f_c becomes more than 1, this means that the neutron scattering effect in the target is increased. We were surprised to find that the contribution of ^{170}Er seemed to widely off in this energy region, however, our test results for the target isotope (see Table II) show that the sample was not oddly devoid of ^{170}Er. We recommend a separate further measurement of the neutron capture cross section of ^{170}Er. From the original yield spectrum in Fig. 5, it can be seen that the thickness of the target at this wide resonance has reached saturation, so the resonance peak has a flat top phenomenon, which results in the broadening of the resonance peak. After the correction of f_c, the contribution of the third resonance of ^{162}Er is shown. It can be ruled out from Table I that the above abnormal conditions originate from impurities.

From the resonance peak fitting, we can see that the resonance peak of the natural erbium in the energy region of 1–100 eV is mostly contributed by the ^{167}Er and ^{162}Er isotopes, although their abundance is not the largest. What is interesting is that most of the discrepancies in the experiment that did not match expectations were related to ^{162}Er. ^{162}Er is the *p* nuclei in astrophysics. Its resonance structure is significant for astrophysics. Therefore, it is necessary to use the high-purity isotope ^{162}Er for fine measurement and analysis.

V. SUMMARY AND CONCLUSIONS

We measured the neutron capture cross section of the natural erbium target in the 1 eV–100 keV energy region at the Back-n facility. The data in the 10–100 keV energy range is used to verify the correctness of the experimental method and data processing. Data in the 100 eV–10 keV energy range can only publish experimental values without giving an accurate uncertainty. The data of the energy region of 1–100 eV

TABLE IV. Resonance parameters extracted from the *R*-matrix analysis of experimental data.

										ENDF/B-VIII.0	
$E_{\text{Experiment}}$(eV)	$E_{\text{Resonance}}$(eV)	Mass	abundance (%)	I	l	J	g	Γ_γ(meV)	Γ_n(meV)	Γ_γ(meV)	Γ_n(meV)
6.00	5.73	162.00	0.139	0.00	0.00	0.50	1.00	103.12	0.36	100.00	0.33
	6.00	167.00	22.869	3.50	0.00	3.00	0.44	95.61	20.32	103.00	20.69
	7.75	162.00	0.139	0.00	0.00	0.50	1.00	99.46	0.58	100.00	0.60
7.95	7.94	167.00	22.869	3.50	0.00	4.00	0.56	89.62	0.12	98.80	0.17
	7.85	164.00	1.606	0.00	0.00	0.50	1.00	84.69	0.59	96.00	0.75
9.29	9.39	167.00	22.869	3.50	0.00	3.00	0.44	67.38	9.30	88.30	9.20
14.63	14.63	162.00	0.139	0.00	0.00	0.50	1.00	111.40	2.80	100.00	4.10
15.55	15.55	166.00	33.503	0.00	0.00	0.50	1.00	88.61	1.93	94.00	2.20
20.22	20.29	162.00	0.139	0.00	0.00	0.50	1.00	100.42	8.28	100.00	8.30
	20.22	167.00	22.869	3.50	0.00	4.00	0.56	100.38	4.52	88.00	4.62
21.98	21.98	167.00	22.869	3.50	0.00	3.00	0.44	123.11	1.40	87.00	1.30
26.27	26.27	167.00	22.869	3.50	0.00	3.00	0.44	102.22	108.60	92.00	94.86
27.41	27.41	167.00	22.869	3.50	0.00	4.00	0.56	116.09	9.96	84.00	10.49
30.42	30.46	164.00	1.606	0.00	0.00	0.50	1.00	104.42	2.25	96.00	4.10
32.88	32.88	167.00	22.869	3.50	0.00	4.00	0.56	108.78	6.77	91.00	6.76
34.82	35.47	162.00	0.139	0.00	0.00	0.50	1.00	105.19	3.13	100.00	5.10
37.5	37.59	167.00	22.869	3.50	0.00	4.00	0.56	124.49	7.31	82.00	7.11
39.44	39.44	167.00	22.869	3.50	0.00	3.00	0.44	138.84	6.95	90.00	8.91
42.22	42.22	167.00	22.869	3.50	0.00	3.00	0.44	151.63	3.16	100.00	3.89
44.51	43.25	162.00	0.139	0.00	0.00	0.50	1.00	101.47	2.12	100.00	2.20
45.85	45.85	162.00	0.139	0.00	0.00	0.50	1.00	105.45	18.68	100.00	19.50
49.61	49.61	164.00	1.606	0.00	0.00	0.50	1.00	105.49	4.35	96.00	4.00
50.18	50.18	167.00	22.869	3.50	0.00	4.00	0.56	135.49	7.30	83.00	6.93
53.60	53.60	167.00	22.869	3.50	0.00	4.00	0.56	126.51	49.16	97.00	48.00
	53.80	164.00	1.606	0.00	0.00	0.50	1.00	95.12	2.42	96.00	2.30
56.57	56.57	164.00	1.606	0.00	0.00	0.50	1.00	103.47	3.42	96.00	6.60
	57.02	162.00	0.139	0.00	0.00	0.50	1.00	101.50	12.95	100.00	32.00
59.92	59.92	167.00	22.869	3.50	0.00	3.00	0.44	143.33	15.00	92.00	14.86
62.12	62.12	167.00	22.869	3.50	0.00	4.00	0.56	118.34	5.38	88.00	5.69
62.79	62.79	167.00	22.869	3.50	0.00	3.00	0.44	112.59	6.68	88.00	7.09
66.05	67.80	162.00	0.139	0.00	0.00	0.50	1.00	100.60	2.55	100.00	3.10
69.40	69.40	167.00	22.869	3.50	0.00	4.00	0.56	122.14	2.32	102.00	2.31
73.79	73.79	166.00	33.503	0.00	0.00	0.50	1.00	111.32	24.96	76.00	65.00
73.84	73.84	167.00	22.869	3.50	0.00	4.00	0.56	96.15	5.40	88.00	5.69
75.69	75.69	167.00	22.869	3.50	0.00	4.00	0.56	93.33	0.96	88.00	1.05
79.28	79.28	167.00	22.869	3.50	0.00	3.00	0.44	102.07	10.49	88.00	11.43
79.74	79.74	168.00	26.940	0.00	0.00	0.50	1.00	100.32	31.18	80.00	41.00
81.73	81.73	166.00	33.503	0.00	0.00	0.50	1.00	128.27	6.14	82.00	9.50
85.50	85.50	167.00	22.869	3.50	0.00	3.00	0.44	90.06	1.33	88.00	1.42
91.33	91.33	167.00	22.869	3.50	0.00	4.00	0.56	100.12	3.12	88.00	3.02
94.45	94.45	167.00	22.869	3.50	0.00	4.00	0.56	82.30	10.41	80.00	17.07
97.38	97.38	167.00	22.869	3.50	0.00	4.00	0.56	88.77	0.94	88.00	0.85
98.02	98.02	167.00	22.869	3.50	0.00	4.00	0.56	87.97	0.22	88.00	0.21

were analyzed in detail and a relatively accurate uncertainty was provided. At the same time, the *R* matrix program is used to provide the isotope contribution of the natural erbium resonance peak and the corresponding resonance parameters. The results show that ^{162}Er, ^{164}Er, and ^{167}Er isotopes have a greater influence on the resonance peak of natural erbium in the 1–100 eV energy region. This work has supplemented and perfected the vacancy in the measurement data of the neutron capture cross section of the natural erbium in the 1–100 eV energy region. Some experimental measurements of the resonance peak parameters and the ENDF evaluation database are different. This work provide an important reference and test for further experimental study of erbium isotopes.

Finally, we noticed that there are some possible weak resonance peak differences between the ^{162}Er isotope experimental measurement and evaluation database. Due to the interference of the environmental background and the resonance peak of the neutron source energy spectrum, a detailed analysis is impossible. We recommend taking further experimental studies for the neutron capture cross section of isotopes of erbium, in particular, the ^{162}Er isotope. At the same time, more accurate neutron source energy spectrum and detailed

background measurement can significantly improve the neutron capture cross section and nuclear astrophysics neutron capture rate research.

ACKNOWLEDGMENTS

We appreciate useful communications from Prof. Gui-Lin Zhang at SINAP and effective technical support from Dr. Yi-Jie Wang at Tsinghua University, Wen-Yi Huang at HUST, and Jun-Wen Wang at Shanghai Tech University. We also greatly appreciate the efforts of the staff of the CSNS and Back-n collaboration. This work was supported by the National Natural Science Foundation of China under Grants No. 11875311, No. 11905274, No. 11605097, and No. 11705156 and the Strategic Priority Research Program of the CAS (No. XDB34030000).

[1] R. Reifarth, C. Lederer, and F. Käppeler, J. Phys. G **41**, 053101 (2014).
[2] F. Thielemann *et al.*, Prog. Part. Nucl. Phys. **66**, 346 (2011).
[3] T. Rauscher *et al.*, Rep. Prog. Phys. **76**, 066201 (2013).
[4] W. A. Fowler, Rev. Mod. Phys. **56**, 149 (1984).
[5] A. Arcones and G. F. Bertsch, Phys. Rev. Lett. **108**, 151101 (2012).
[6] A. Bartlett, J. Gorres, G. J. Mathews, K. Otsuki, M. Wiescher, D. Frekers, A. Mengoni, and J. Tostevin, Phys. Rev. C **74**, 015802 (2006).
[7] J. Y. Tang *et al.*, At. Energy Sci. Technol. **53**, 2012 (2019).
[8] H. Beer, F. Kaeppeler, K. Wisshak, and R. A. Ward, Astrophys. J. **46**, 295 (1981).
[9] J. R. D. Lepine *et al.*, Nucl. Phys. **196**, 83 (1972).
[10] J. H. Gibbons *et al.*, Phys. Rev. **122**, 182 (1961).
[11] L. Koester and K. Knopf, Z. Phys. A **323**, 367 (1986).
[12] H. Chen and X. L. Wang, Nat. Mater. **15**, 689 (2016).
[13] J. B. Yu *et al.*, Nucl. Sci. Tech. **28**, 46 (2017).
[14] X. M. Jin *et al.*, Nucl. Sci. Tech. **30**, 143 (2019).
[15] R. Xiao *et al.*, Nucl. Sci. Tech. **28**, 109 (2017).
[16] Q. An, H. Y. Bai, J. Bao *et al.*, J. Instrum. **12**, P07022 (2017).
[17] Q. L. Mu *et al.*, Nucl. Tech. **42**, 120502 (2019).
[18] J. Y. Tang *et al.*, Chin. Phys. C **34**, 121 (2010).
[19] J. Ren, X. Ruan, and J. Bao, Radiat. Detect. Technol. Methods **3**, 52 (2019).
[20] Q. Li, G. Luan, J. Bao *et al.*, Nucl. Instrum. Methods Phys. Res. A **946**, 162497 (2019).
[21] Q. Wang, P. Cao, X. Qi *et al.*, Rev. Sci. Instrum. **89**, 013511 (2018).
[22] J. Ren *et al.*, Nucl. Instrum. Methods Phys. Res. A **985**, 164703 (2021).
[23] X. X. Li *et al.*, Nucl. Tech. **43**, 80501 (2020).
[24] J. H. Gibbons and R. L. Macklin, Science **156**, 1039 1967).
[25] A. Borella, G. Aerts, F. Gunsing *et al.*, Nucl. Instrum. Methods Phys. Res. A **577**, 626 (2007).
[26] R. L. Macklin and J. H. Gibbons, Phys. Rev. **159**, 1007 (1967).
[27] J. Ren, Ph.D thesis, China Institute of Atomic Energy, Beijing, China (2018).
[28] C. Massimi *et al.* (n-TOF Collaboration), Phys. Rev. C **81**, 044616 (2010).
[29] S. Agostinelli *et al.* (Geant4 Collaboration), Nucl. Instrum. Methods Phys. Res. A **506**, 250 (2003).
[30] Y. H. Chen *et al.*, Eur. Phys. J. A **55**, 115 (2019).
[31] J. L. Tain *et al.*, J. Nucl. Sci. Technol. **39**, 689 (2002).
[32] J. Ren *et al.*, Acta Phys. Sin. **69**, 172901 (2020).
[33] R. W. Hockenbury *et al.*, Phys. Rev. **178**, 1746 (1969).
[34] N. M. Larson, Oak Ridge National Laboratory, Report No. ORNL/TM-9179/R7, 2006.
[35] S. F. Mughabghab, *Neutron Cross Sections: Neutron Resonance Parameters and Thermal Cross Sections* (Academic Press, New York, 2006).
[36] A. Gawlik *et al.* Phys. Rev. C **100**, 045804 (2019).